




COVID-19

Design of a Microfluidic Bleeding Chip to Evaluate Antithrombotic Agents for Use in COVID-19 Patients

HARI HARA SUDHAN LAKSHMANAN ¹, ADITYA A. PORE,² TIA C. L. KOHS,¹ FEYZA YAZAR,³ RACHEL M. THOMPSON,¹ PATRICK L. JURNEY,³ JEEVAN MADDALA,¹ SVEN R. OLSON,^{1,4} JOSEPH J. SHATZEL,^{1,4} SIVA A. VANAPALLI,² and OWEN J. T. MCCARTY^{1,4}

¹Department of Biomedical Engineering, Oregon Health & Science University, 3303 SW Bond Ave; CH13B, Portland, OR 97239, USA; ²Department of Chemical Engineering, Texas Tech University, Lubbock, TX, USA; ³Department of Biomedical Engineering, San José State University, San Jose, CA, USA; and ⁴Division of Hematology & Medical Oncology, School of Medicine, Oregon Health & Science University, Portland, OR, USA

(Received 8 June 2020; accepted 31 July 2020; published online 6 August 2020)

Associate Editor Owen J. T. McCarty oversaw the review of this article.

Abstract

Introduction—Interventions that could prevent thrombosis, clinical decompensation, and respiratory compromise in patients with novel coronavirus disease (COVID-19) are key to decrease mortality rate. Studies show that profound cytokine release and excessive activation of blood coagulation appear to be key drivers of COVID-19 associated mortality. Since limited *in vitro* methods exist for assessing the effects of anticoagulants on hemostasis, the development of novel therapies to safely prevent thrombosis in COVID-19 patients relies on preclinical animal models and early phase human trials. Herein we present the design of a microfluidic “bleeding chip” to evaluate the effects of antithrombotic therapies on hemostatic plug formation *in vitro*.

Methods—The design of the microfluidic device consists of two orthogonal channels: an inlet that serves as a model blood vessel, and a bleeding channel to model hemostatic plug formation at sites of compromised endothelial barrier function. This is achieved by placing a series of 3 pillars spaced 10 μm apart at the intersection of the two channels. The pillars and bleeding channel are coated with the extracellular matrix protein collagen.

Results—Perfusion of human whole blood through the microfluidic bleeding chip led to initial platelet adhesion and aggregation at the pillars followed by hemostatic plug formation and occlusion of the bleeding channel.

Conclusions—Safe and effective mitigating agents are needed for treatment and prevention of thrombotic complications in COVID-19 patients. This simple microfluidic device holds

potential to be developed into a tool for assessing the effects of anticoagulant therapy on hemostasis.

Keywords—Platelets, Microfluidics, Hemostasis, Thrombosis, Anticoagulant, Antithrombotic, COVID-19.

ABBREVIATIONS

BSA	Bovine serum albumin
CAS	Contact activation system
COVID-19	Coronavirus disease-19
DIC	Differential interference contrast
FX	Coagulation factor X
LMWH	Low molecular weight heparin
PBS	Phosphate buffer saline
PDMS	Polydimethylsiloxane
SARS-CoV-2	Severe acute respiratory syndrome coronavirus 2
vWF	von Willebrand factor

INTRODUCTION

Coronavirus disease 19 (COVID-19) caused by severe acute respiratory syndrome coronavirus 2 (SARS-CoV-2) infection is a global pandemic, having infected nearly 13 million around the world by the time of this writing. Primarily a respiratory disease, COVID-19 patients with severe infection suffer from inflammatory and thrombotic complications.^{6,34} A retrospective analysis of COVID-19 patients revealed

Address correspondence to Hari Hara Sudhan Lakshmanan, Department of Biomedical Engineering, Oregon Health & Science University, 3303 SW Bond Ave; CH13B, Portland, OR 97239, USA. Electronic mail: lakshmah@ohsu.edu

Hari Hara Sudhan Lakshmanan and Aditya A. Pore are Co-first authors.

that 71.4% of patients who died developed disseminated intravascular coagulation (DIC) compared to only 0.6% of survivors.³⁰ Critically ill COVID-19 patients have been found to frequently develop thrombotic manifestations including microvascular thrombosis, venous thromboembolism, and acute arterial thrombosis. Despite standard prophylactic anticoagulant administration the rate of thrombosis approach 20% in hospitalized patients.^{2,5,8,19,32} While heparin is a convenient and biologically plausible attractive anticoagulant for COVID-19 due to its potential anti-inflammatory, anti-complement, and even direct antiviral effects, the persistently high rate of thromboembolic disease despite routine heparin use implies an urgent unmet need for alternative agents.^{11,22,25} Several direct and indirect mechanisms have been proposed by which SARS-CoV-2 infection induces pathologic upregulation of inflammation and coagulation, as illustrated in Fig. 1. This has led to significant enthusiasm for mobilizing clinical trials targeting either pathway, balancing efficacy with safety. With regards to developing novel anticoagulants for treatment of COVID-19 patients, this demands that

these strategies ensure hemostatic safety, i.e. no abnormal bleeding. While the most clinically relevant conclusions regarding the safety of anticoagulants will ultimately be learned through clinical trials, *in vitro* models hold potential usefulness in revealing early safety and efficacy signals to guide future anticoagulant development of agents to prevent thrombosis in COVID-19 patients without compromising hemostasis.

The key mechanisms that drive intravascular thrombus formation in diseased vascular beds were elucidated in part due to the creation and use of *in silico*, *in vitro*, *ex vivo* and *in vivo* models of thrombus formation under shear flow.^{7,13,16} Building upon this knowledge, a number of antithrombotic agents targeting either platelets or the coagulation cascade have been brought to market for use in the prevention or treatment of cardiovascular diseases including heart attack and stroke. Yet, despite advances in identifying targets to improve the efficacy of antithrombotic therapy, *in vitro* models to predict clinical bleeding are limited. This is particularly relevant in COVID-19, as new antithrombotic agents including inhibitors of platelet function, coagulation factor (*F*) *X*, or the

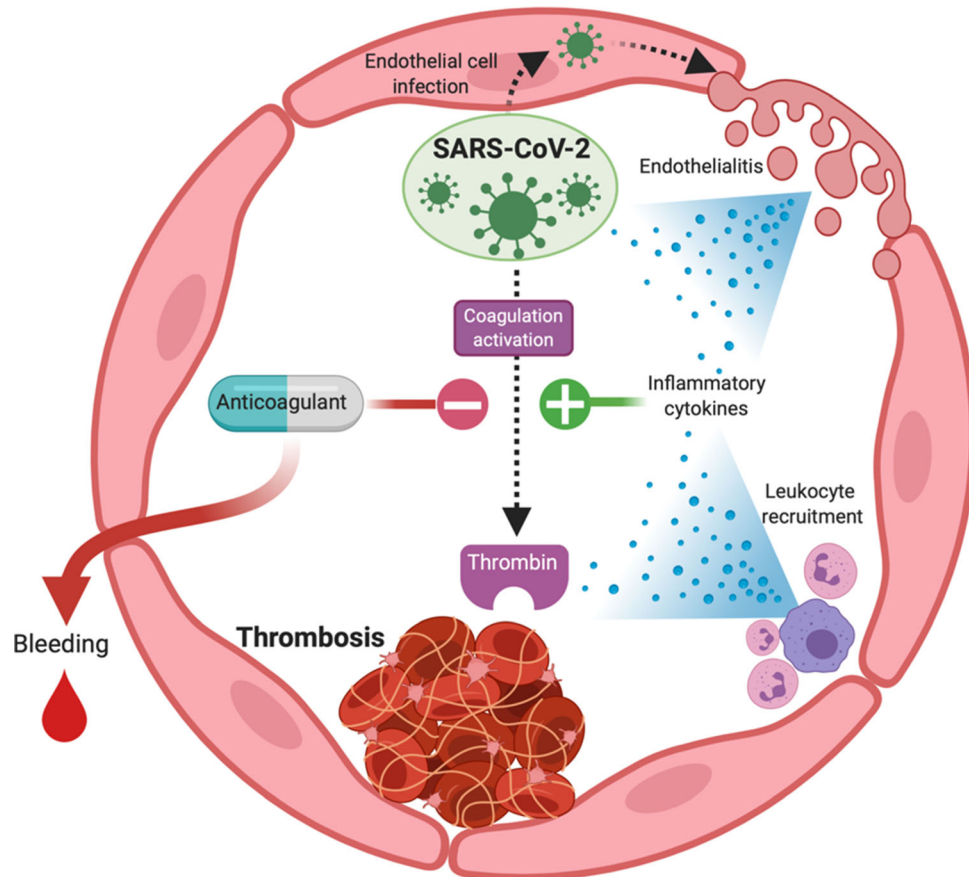


FIGURE 1. Hypothesized procoagulant mechanisms of SARS-CoV-2 infection including endothelialitis, leukocyte recruitment, inflammatory cytokine release and direct activation of coagulation enzymes. Use of anticoagulants to block the development of COVID-related thrombosis must take into account their potential to incite pathologic bleeding.

contact activation system will likely have to be used in combination with heparin as a standard-of-care therapy.²⁸ An understanding of any potentially deleterious effects of such drug combinations on hemostasis will have to await the results of ongoing or proposed early phase clinical trials. This is due in part to the fact that the physical biology and rheology underlying hemostatic plug formation are ill-defined relative to our understanding of thrombosis.⁹

The events that support hemostasis (extravascular) vs. thrombosis (intravascular) are distinct in part due to the rheology of blood flow that differentially distributes blood constituents inside and outside blood vessels. Several elegant microfluidic models of the hemostatic response to a mechanical injury of the microvasculature have recently been developed.^{26,27} Here we extend these models based on the percolation theory of fluid dynamics to develop a model of blood transport into the tissue space at sites of compromised endothelial cell barrier function, such as in inflamed tissue beds and other forms of microangiopathy.³ To achieve this, we present the design of a microfluidic device with two orthogonal channels: a main channel that serves as a model blood vessel, and a bleeding channel to model hemostatic plug formation. We propose this model could be utilized to identify potential anticoagulant and antithrombotic targets and test agents to mitigate the thrombotic complications associated with COVID-19 whilst preserving hemostasis.

MATERIALS AND METHODS

The design consists of two orthogonal channels: a main channel of width 150 μm , length 10 mm and a side channel of width 100 μm , length 3 mm as shown in Fig. 2a. We designed 3 circular pillars of diameter 20 μm , placed 10 μm apart at the intersection of two channels. All features have a uniform height of 50 μm . One side of the main channel serves as the inlet for blood, referred to as the *inlet channel* and the side channel with the pillars is termed the *bleeding channel* as indicated in Fig. 2a. Only the bleeding channel is functionalized with fibrillar collagen to represent the subendothelial extracellular matrix. This method can be modified to include coating the bleeding channel with tissue factor alone or in combination with extracellular matrix proteins including collagen, nidogen, or laminin.^{15,37} The gaps in the pillars represent compromised endothelial barrier function as a result of inflammation or vascular injury. The physical parameters of the pillars including number, radius, and spacing could be modified to study the effects of the physical biology of barrier function on the kinetics of hemostatic plug formation.

The design for the bleeding chip was drawn in AutoCAD and was printed on photomask (CAD/Art Services Inc., Oregon, USA). Standard soft-lithography techniques were used for making the bleed chip.^{23,35} The master mold was a single layer design, fabricated using a negative photoresist SU-8 2050 (Kayaku Advanced Materials, USA) with feature height of 50 μm . Microfluidic devices were made by mixing polydimethylsiloxane (PDMS) (Sylgard 184, Dow Corning, USA) monomer and the curing agent in a 10:1 ratio followed by degassing of the solution, pouring it over the master mold and curing it at 70 $^{\circ}\text{C}$ for 2 h. After curing, the PDMS replicas were cut and peeled from the SU-8 mold. Fluid inlets and outlets were punched using a 1 mm biopsy punch (Miltex, Japan). The PDMS replicas were bonded to a cover glass (Thermo Scientific, USA) of thickness 170 μm , after plasma treating (Harrick Plasma, Ithaca, New York) the surfaces for 90 s. This assembly was baked at 70 $^{\circ}\text{C}$ for 4 mins to strengthen the bonding.

To coat the bleeding channel with fibrillar collagen (100 $\mu\text{g mL}^{-1}$, Chronolog), a collagen droplet of 2 μL volume was introduced by pipette into the bleeding channel; the leading edge of the droplet meniscus was advanced until the collagen solution reached the pillars as observed with a 10 \times microscope objective. Capillary forces were sufficient to restrict the collagen solution from entering the orthogonal vessel channel, thus allowing selective coating of the bleeding channel and pillars with collagen as shown in Fig. 2b. After an hour of incubation at room temperature, both channels were washed with phosphate buffer saline (PBS) and blocked with 5 mg mL^{-1} denatured bovine serum albumin (BSA) for 1 h followed by washing with PBS. Relevant controls would include coating the bleeding channel with BSA.

Human venous blood was collected from healthy adult volunteers into a syringe filled with 3.8% sodium citrate (1/10th blood volume) in accordance with the Oregon Health & Science University Institutional Review Board. Citrated blood was recalcified with the addition of (1:9 recalcification buffer: blood) recalcification buffer (75 mmol L^{-1} CaCl_2 and 37.5 mmol L^{-1} MgCl_2), to allow for coagulation. This method could be modified for use with reconstituted blood (purified red blood cells, platelets, and plasma) to allow for parameters such as platelet count to be adjusted. Recalcified blood was loaded into a 1 mL syringe and assembled onto a Harvard 2000 syringe pump as shown in Fig. 3. The syringe was connected to the device inlet with a 0.5 mm polyethylene tubing (Braintree scientific, USA) and the blood was perfused at a constant flow rate of 10 $\mu\text{L min}^{-1}$, which corresponds to an arterial shear rate of 1000 s^{-1} in the inlet channel. The outlet of the bleeding channel was con-

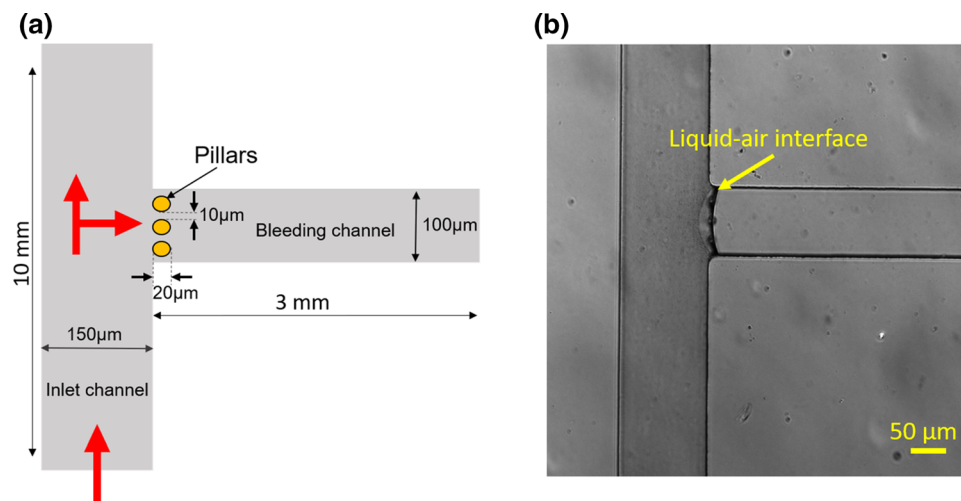


FIGURE 2. Design and development of a polydimethylsiloxane based microfluidic bleed chip. (a) The bleed chip consists of an inlet channel of width $150\ \mu\text{m}$, length $10\ \text{mm}$ and a side channel of width $100\ \mu\text{m}$, length $3\ \text{mm}$ referred to as the *bleeding channel*. At the intersection of channels, there are 3 pillars of $20\ \mu\text{m}$ diameter with a $10\ \mu\text{m}$ gap between them. Red arrows depict the direction of blood flow in the device (Figure not to scale). (b) Differential interference contrast (DIC) $10\times$ image of the device where the bleeding channel is coated with fibrillar collagen ($100\ \mu\text{g mL}^{-1}$). The arrow indicates the liquid-air interface during coating of the bleeding channel. Scale: $50\ \mu\text{m}$

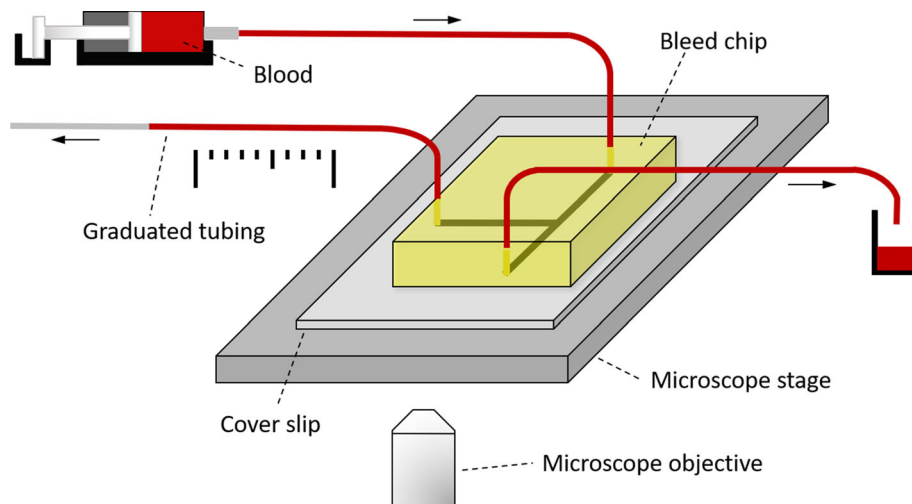


FIGURE 3. Experimental setup for the use of bleed chip with blood sample. Device inlet is connected to a syringe pump with a syringe filled with recalcified whole human blood. The bleeding channel is connected to a $0.5\ \text{mm}$ polyethylene tube with graduations every $0.5\ \text{cm}$ to record the blood flow rate through the bleeding channel. An equal length of polyethylene tubing is connected to the second outlet leading to waste collection. Real time dynamics of blood flow inside the bleed chip is captured with the $10\times$ objective of a DIC Zeiss Axio Imager 2 microscope. Arrows denote the direction of blood flow.

nected with polyethylene tubing ($20\ \text{cm}$ length) graduated every $0.5\ \text{cm}$ to record the velocity of blood flow in the bleeding channel. The main channel outlet was also connected to polyethylene tubing of similar length for waste collection. Platelet adhesion, aggregation and thrombus formation in the device near the pillars during blood perfusion was recorded using Kohler illuminated Nomarski differential interference contrast (DIC) optics with a Zeiss $10\times$ lens on a Zeiss Axio Imager M2 microscope (Carl Zeiss MicroImaging GmbH, Germany). Graduations in the polyethylene

tubing connected to the bleeding channel enabled manual monitoring and recording of blood velocity and volume in the bleeding channel.

RESULTS AND DISCUSSION

We performed computational fluid dynamic simulations using a 2D model of the bleeding chip created in COMSOL to predict the hemodynamics at and near the interface created by the pillars. Our model included

the constant flow rate of $10 \mu\text{L min}^{-1}$ at the inlet, a constant atmospheric pressure at the main channel outlet and a constant flow rate of $2 \mu\text{L min}^{-1}$ at the bleeding channel outlet. Blood was modeled as a non-Newtonian fluid using power-law as described in the literature.³⁶ Our initial model was based on the average physical parameters of density and viscosity of human whole blood and did not take into account changes in these parameters due to the addition of anticoagulants, recalcification buffer, or differences in donor hematocrit. Based on the inlet flow rate, we estimated a Reynold's number (Re) ≈ 0.5 for flow in the device resulting in an assumption of creeping flow inside the device. Although the low Re flow in the model may not capture the physiology of blood flow, this is a limitation associated with the field of microfluidics in general and there remains a need for scaling approaches that better relate the rheology observed in microfluidic models to the biophysical parameters of veins, capillaries and arteries. The Navier–Stokes equation for creeping flow was solved using COMSOL under steady state conditions to create velocity and shear rate profiles as shown in Figs. 4a and 4b. Velocity profiles derived from the microfluidic device indicated a series of stagnation points along the pillar surface and the corners at the channel intersection (Fig. 4a). Platelet aggregation at stagnation points has been shown to initiate a core and shell thrombus wherein the core consists of procoagulant platelets which facilitates localized thrombin generation whereas the shell is comprised of weakly activated platelets which acts as a rheological shield.^{12,29} For our bleeding chip model,

the shear rate profile shows a change in shear rate from 1000 s^{-1} in the inlet channel to 9000 s^{-1} in the spaces between the pillars of the bleeding channel, thus introducing a shear gradient. This region of increasing shear rate was followed by decreasing shear rates in the bleeding channel downstream of the pillars as shown in Fig. 4b. Rapid transition of shear rate over short distances has been shown to promote platelet activation and aggregation due to platelet GPIb-von Willebrand factor (vWF) interaction.²¹ The Peclet number (Pe) $\gg 1$ for the transport of zymogens from bulk flow to the pillar surface at steady state conditions implies a significant dependence on advection as the primary transport mechanism.^{4,17}

We experimentally observed the initiation and propagation of hemostatic plug formation at the sites predicted by our computational model as “locations of shear gradients”. The dynamics of hemostatic plug formation were imaged by DIC microscopy. Figure 5a shows the progression of platelet aggregation and coagulation around the pillars at the entrance of bleeding channel at 0, 5, and 10 min perfusion times. Hemostatic plug formation was observed to initiate at and around the pillars as indicated by the dotted circle in Fig. 5a. The growth of the hemostatic plug continued in the direction of flow inside the bleeding channel over the next 5 min. By 10 min a patent hemostatic plug was formed and blood flow ceased. In contrast, in the absence of coagulation using sodium citrate-anticoagulated whole blood, hemostatic plug formation was incapable of stopping blood flow in the bleeding channel. At present the time to occlusion is a labora-

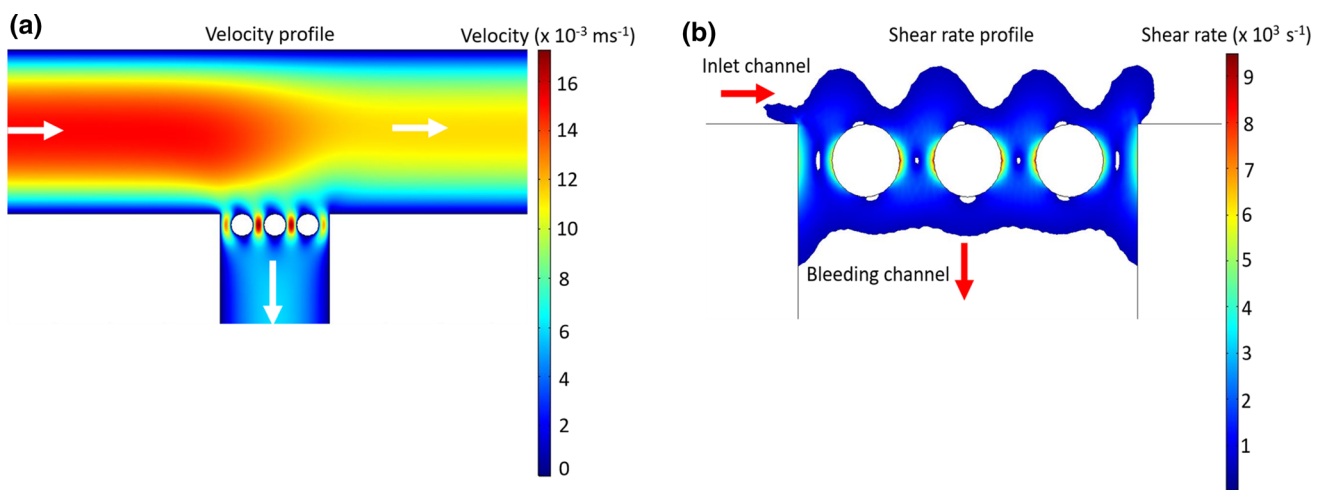


FIGURE 4. Estimation of shear rate and velocity in the bleed chip using numerical modeling. Computational fluid dynamics model of the bleed chip was solved using COMSOL to generate surface plots of velocity (a) and shear rate (b) in the bleed chip at initial steady state conditions. (a) Surface plot of velocity in the bleed chip at steady state conditions. White arrows indicate the direction of flow in the device. Blood is modeled as a non-Newtonian power law fluid and the Navier–Stokes equation is solved using COMSOL to compute the velocity and shear rate in the bleed chip at steady state conditions. (b) Wall shear rate increases from 1000 s^{-1} in the main channel to 9000 s^{-1} on pillar surfaces and then decreases to 1000 s^{-1} distal to the pillars in the bleeding channel.

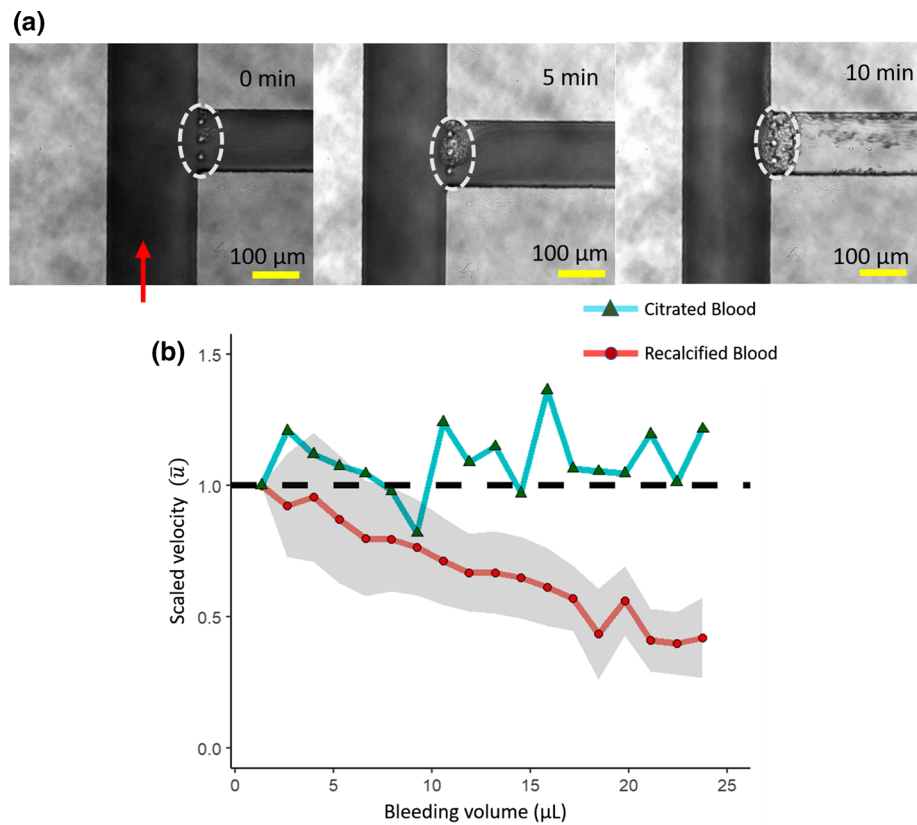


FIGURE 5. Dynamics of blood flow and hemostatic plug formation in the bleed chip. Human whole blood, with or without recalcification, was perfused through the bleed chip at a constant flow rate of $10 \mu\text{L min}^{-1}$ using syringe pump. The dynamics of hemostatic plug formation in the pillar region was recorded through $10\times$ DIC microscope (a) and the velocity of blood in the bleeding channel was recorded through a graduated tubing connected to the bleeding channel outlet and transformed into scaled velocity (b). (a) $10\times$ DIC images of the pillar region of the bleed chip at 0, 5 and 10 min after perfusion of recalcified whole human blood at a constant inlet flow rate of $10 \mu\text{L min}^{-1}$. Red arrow depicts the direction of blood flow in the device and the white ellipse with broken lines indicates the pillar region. Scale: $100 \mu\text{m}$. (b) Scaled velocity of blood (\bar{u}) as a function of volume of blood in the bleeding channel. Scaled velocity ($\bar{u} = \frac{u_i}{u_0}$) is the ratio of blood velocity at a given time point (u_i) to the initial blood velocity (u_0) measured in the bleeding channel. Dashed line indicates a scaled velocity (\bar{u}) of 1.0. Errors are \pm standard error of means for four trials.

tory-based experimental parameter, akin to a clotting time in an APTT assay; future studies are required to relate this parameter to the kinetics of hemostatic plug formation at sites of vascular injury or compromised barrier function and relevant scaling of the model to vascular beds, veins and arteries.

The velocity of blood in the bleeding channel was recorded by quantifying the rate of blood flow within a graduated polyethylene tubing connected to the distal end of bleeding channel. We report the scaled velocity (\bar{u}) = $\frac{u_i}{u_0}$ in Fig. 5b where u_i is the velocity of blood measured at a given time point and u_0 is the initial velocity of blood measured in the tubing connected to the bleeding channel. Our pilot data show a reduction in blood flow velocity as a function of time. Of note, we observed fluctuations in scaled velocity due to ‘re-bleeding’ wherein a portion of the hemostatic plug would become unstable and erode in a similar manner as has been observed in animal models of hemostatic

plug formation.^{31,33} Our current technique to measure velocity of blood in the bleeding channel is limited to the granularity of measuring discrete time intervals associated with $1.3 \mu\text{L}$ gradations in blood volume; continuous monitoring of the blood volume and velocity with techniques including gravimetric or doppler measurements of volumetric flow rate would improve the precision of this platform, albeit at an increased cost of design.

This method can be developed to study hemostasis *in vitro* under physiologically relevant flow conditions. The effect of inhibitors of the intrinsic, extrinsic and common pathways of coagulation alone or in combination with anti-platelets inhibitors including PAR4 and P2Y12 antagonists on hemostatic plug formation can readily be evaluated in this model.^{20,24} The sensitivity of this model to changes in platelet count and hematocrit remain to be validated.

Translation for Use in COVID-19

The primary cause of death in COVID-19 is progressive respiratory failure, which has been increasingly associated with the presence and frequency of microangiopathy thrombi in the pulmonary vessels of COVID-19 patients.^{10,18} For instance, reports have shown the rate of alveolar capillary microthrombi were nearly 9-fold higher in COVID-19 patients as compared to patients with influenza.¹ In the intensive care unit, cumulative incidence rates nearing 50% have been reported for arterial and venous thrombosis in COVID-19 patients despite the widespread adoption of low molecular weight heparin (LMWH) as primary thromboprophylaxis.^{14,19} These observations highlight both the need for novel safe and effective antithrombotic strategies to combat thrombosis in COVID-19 patients, as well as our lack of understanding of the pathology of thrombosis in infectious diseases including COVID-19. Novel anticoagulant strategies such as inhibitors of the contact activation system (CAS) of coagulation and stimulators of the protein C pathway will likely see introduction into clinical trials in combination with heparin products.²⁸ As LMWH is known to compromise hemostasis, combinations of novel anticoagulants with LMWH will require careful study to ensure no compounding effects on hemostasis. The development of *in vitro* or *ex vivo* models of hemostasis may be useful in predicting the potential for adverse major bleeding events for the use of novel anticoagulants as monotherapy or in combination with LMWH prior to evaluation in clinical trials. Herein we describe the development of a simple microfluidic-based assay to model hemostasis. We aim to use this model for evaluation and dose selection of CAS inhibitors for use in clinical trials to evaluate their safety and efficacy in mitigating thrombosis in COVID-19.

AUTHOR CONTRIBUTIONS

HHSL, AAP, JJS, JM, SAV, PJ, and OJTM conceived and designed the research. HHSL, RMT, AAP, PJ and FY performed experiments and modeling. HHSL, JM, JJS, AAP, SAV, PJ and OJTM interpreted experimental and modeling data. HHSL, AAP, SRO and FY prepared the figures. HHSL, TCLK and OJTM drafted the manuscript. HHSL, AAP, JJS, JM, SRO, TCLK, PJ, SAV and OJTM revised and edited the manuscript. HHSL, AAP, JJS, JM, SRO, TCLK, RMT, FY, PJ, SAV and OJTM approved the final version of the manuscript.

ACKNOWLEDGMENTS

This work was supported by grants from the National Institutes of Health (R01HL101972 and R01HL144113) and the American Heart Association (18UFEL33960363). R.M. Thompson is an AHA Undergraduate Research Fellow.

CONFLICT OF INTEREST

HH.S. Lakshmanan, A.A. Pore, T.C.L. Kohs, F. Yazar, R.M. Thompson, P.L. Journey, J. Maddala, S.R. Olson, J.J. Shatzel, S.A. Vanapalli and O.J.T. McCarty declare no conflict of interest.

RESEARCH INVOLVING HUMAN AND ANIMAL RIGHTS

All human subjects research was carried out in accordance with institutional guidelines approved by the Oregon Health & Science University Institutional Review Board. No animal studies were carried out by the authors for this article.

REFERENCES

- ¹Ackermann, M., S. E. Verleden, M. Kuehnel, A. Haverich, T. Welte, F. Laenger, A. Vanstapel, C. Werlein, H. Stark, A. Tzankov, W. W. Li, V. W. Li, S. J. Mentzer, and D. Jonigk. Pulmonary vascular endothelialitis, thrombosis, and angiogenesis in Covid-19. *N. Engl. J. Med.* 383(2):120–128, 2020.
- ²Bikdeli, B., M. V. Madhavan, D. Jimenez, T. Chuich, I. Dreyfus, E. Driggin, C. Nigoghossian, W. Ageo, M. Madjid, Y. Guo, L. V. Tang, Y. Hu, J. Giri, M. Cushman, I. Quere, E. P. Dimakakos, C. M. Gibson, G. Lippi, E. J. Favaloro, J. Fareed, J. A. Caprini, A. J. Tafur, J. R. Burton, D. P. Francese, E. Y. Wang, A. Falanga, C. McLintock, B. J. Hunt, A. C. Spyropoulos, G. D. Barnes, J. W. Eikelboom, I. Weinberg, S. Schulman, M. Carrier, G. Piazza, J. A. Beckman, P. G. Steg, G. W. Stone, S. Rosenkranz, S. Z. Goldhaber, S. A. Parikh, M. Monreal, H. M. Krumholz, S. V. Konstantinides, J. I. Weitz, and G. Y. H. Lip. COVID-19 and thrombotic or thromboembolic disease: implications for prevention, antithrombotic therapy, and follow-up. *J. Am. Coll. Cardiol.* 75:2950–2973, 2020.
- ³Bird, R. B., W. E. Stewart, and E. N. Lightfoot. *Transport Phenomena*. New York: Wiley, 1960.
- ⁴Brass, L. F., and S. L. Diamond. Transport physics and biorheology in the setting of hemostasis and thrombosis. *J. Thromb. Haemost.* 14:906–917, 2016.
- ⁵Cattaneo, M., E. M. Bertinato, S. Bircocchi, C. Brizio, D. Malavolta, M. Manzoni, G. Muscarella, and M. Orlandi. Pulmonary embolism or pulmonary thrombosis in COV-

- ID-19? Is the recommendation to use high-dose heparin for thromboprophylaxis justified? *Thromb. Haemost.* 2020. <https://doi.org/10.1055/s-0040-1712097>.
- ⁶Connors, J. M., and J. H. Levy. COVID-19 and its implications for thrombosis and anticoagulation. *Blood.* 135:2033–2040, 2020.
- ⁷Diamond, S. L. Systems analysis of thrombus formation. *Circ. Res.* 118:1348–1362, 2016.
- ⁸Divani, A. A., S. Andalib, M. Di Napoli, S. Lattanzi, M. S. Hussain, J. Biller, L. D. McCullough, M. R. Azarpazhooh, A. Seletska, S. A. Mayer, and M. Torbey. Coronavirus disease 2019 and stroke: clinical manifestations and pathophysiological insights. *J. Stroke Cerebrovasc. Dis.* 104941, 2020.
- ⁹Fogelson, A. L., and K. B. Neeves. Fluid mechanics of blood clot formation. *Annu. Rev. Fluid Mech.* 47:377–403, 2015.
- ¹⁰Gavriilaki, E., and R. A. Brodsky. Severe COVID-19 infection and thrombotic microangiopathy: success does not come easily. *Br. J. Haematol.* 189:e227–e230, 2020.
- ¹¹Hao, C., H. Xu, L. Yu, and L. Zhang. Heparin: an essential drug for modern medicine. *Prog. Mol. Biol. Transl. Sci.* 163:1–19, 2019.
- ¹²Herbig, B. A., and S. L. Diamond. Thrombi produced in stagnation point flows have a core-shell structure. *Cell Mol. Bioeng.* 10:515–521, 2017.
- ¹³Herbig, B. A., X. Yu, and S. L. Diamond. Using microfluidic devices to study thrombosis in pathological blood flows. *Biomicrofluidics.* 12:042201, 2018.
- ¹⁴Klok, F. A., M. Kruip, N. J. M. van der Meer, M. S. Arbous, D. Gommers, K. M. Kant, F. H. J. Kaptein, J. van Paassen, M. A. M. Stals, M. V. Huisman, and H. Endeman. Incidence of thrombotic complications in critically ill ICU patients with COVID-19. *Thromb. Res.* 191:145–147, 2020.
- ¹⁵Lakshmanan, H. H. S., A. R. Melrose, A. I. Sepp, A. Mitrugno, A. T. P. Ngo, A. Khader, R. Thompson, D. Sallee, J. Pang, P. H. Mangin, M. Jandrot-Perrus, J. E. Aslan, and O. J. T. McCarty. The basement membrane protein nidogen-1 supports platelet adhesion and activation. *Platelets* 2020. <https://doi.org/10.1080/09537104.2020>.
- ¹⁶Matafonov, A., P. Y. Leung, A. E. Gailani, S. L. Grach, C. Puy, Q. Cheng, M. F. Sun, O. J. McCarty, E. I. Tucker, H. Kataoka, T. Renne, J. H. Morrissey, A. Gruber, and D. Gailani. Factor XII inhibition reduces thrombus formation in a primate thrombosis model. *Blood.* 123:1739–1746, 2014.
- ¹⁷McCarty, O. J., D. Ku, M. Sugimoto, M. R. King, J. M. Cosemans, and K. B. Neeves. Dimensional analysis and scaling relevant to flow models of thrombus formation: communication from the SSC of the ISTH. *J. Thromb. Haemost.* 14:619–622, 2016.
- ¹⁸McGonagle, D., J. S. O'Donnell, K. Sharif, P. Emery, and C. Bridgewood. Immune mechanisms of pulmonary intravascular coagulopathy in COVID-19 pneumonia. *Lancet Rheumatol.* 2:E437–E445, 2020.
- ¹⁹Middeldorp, S., M. Coppens, T. F. van Haaps, M. Foppen, A. P. Vlaar, M. C. A. Muller, C. C. S. Bouman, L. F. M. Beenen, R. S. Kootte, J. Heijmans, L. P. Smits, P. I. Bonta, and N. van Es. Incidence of venous thromboembolism in hospitalized patients with COVID-19. *J. Thromb. Haemost.* 2020. <https://doi.org/10.1111/jth.14888>.
- ²⁰Mitrugno, A., R. A. Rigg, N. B. Laschober, A. T. P. Ngo, J. Pang, C. D. Williams, J. E. Aslan, and O. J. T. McCarty. Potentiation of TRAP-6-induced platelet dense granule release by blockade of P2Y12 signaling with MRS2395. *Platelets.* 29:383–394, 2018.
- ²¹Nesbitt, W. S., E. Westein, F. J. Tovar-Lopez, E. Tolouei, A. Mitchell, J. Fu, J. Carberry, A. Fouras, and S. P. Jackson. A shear gradient-dependent platelet aggregation mechanism drives thrombus formation. *Nat. Med.* 15:665–673, 2009.
- ²²Onishi, A., K. StAnge, J. S. Dordick, and R. J. Linhardt. Heparin and anticoagulation. *Front Biosci.* 21:1372–1392, 2016.
- ²³Qin, D., Y. Xia, and G. M. Whitesides. Soft lithography for micro- and nanoscale patterning. *Nat. Protoc.* 5:491–502, 2010.
- ²⁴Rigg, R. A., L. D. Healy, T. T. Chu, A. T. P. Ngo, A. Mitrugno, J. Zilberman-Rudenko, J. E. Aslan, M. T. Hinds, L. D. Vecchiarelli, T. K. Morgan, A. Gruber, K. J. Temple, C. W. Lindsley, M. T. Duvernay, H. E. Hamm, and O. J. T. McCarty. Protease-activated receptor 4 activity promotes platelet granule release and platelet-leukocyte interactions. *Platelets.* 30:126–135, 2019.
- ²⁵Sahu, A., and M. K. Pangburn. Identification of multiple sites of interaction between heparin and the complement system. *Mol. Immunol.* 30:679–684, 1993.
- ²⁶Sakurai, Y., E. T. Hardy, B. Ahn, R. Tran, M. E. Fay, J. C. Ciciliano, R. G. Mannino, D. R. Myers, Y. Qiu, M. A. Carden, W. H. Baldwin, S. L. Meeks, G. E. Gilbert, S. M. Jobe, and W. A. Lam. A microengineered vascularized bleeding model that integrates the principal components of hemostasis. *Nat. Commun.* 9:509, 2018.
- ²⁷Schoeman, R. M., K. Rana, N. Danes, M. Lehmann, J. A. Di Paola, A. L. Fogelson, K. Leiderman, and K. B. Neeves. A microfluidic model of hemostasis sensitive to platelet function and coagulation. *Cell Mol. Bioeng.* 10:3–15, 2017.
- ²⁸Shatzel, J. J., E. P. DeLoughery, C. U. Lorentz, E. I. Tucker, J. E. Aslan, M. T. Hinds, D. Gailani, J. I. Weitz, O. J. McCarty, and A. Gruber. The contact activation system as a potential therapeutic target in patients with COVID-19. *Res. Pract. Thromb. Haemost.* 4:500–505, 2020.
- ²⁹Stalker, T. J., E. A. Traxler, J. Wu, K. M. Wannemacher, S. L. Cermignano, R. Voronov, S. L. Diamond, and L. F. Brass. Hierarchical organization in the hemostatic response and its relationship to the platelet-signaling network. *Blood.* 121:1875–1885, 2013.
- ³⁰Tang, N., D. Li, X. Wang, and Z. Sun. Abnormal coagulation parameters are associated with poor prognosis in patients with novel coronavirus pneumonia. *J. Thromb. Haemost.* 18:844–847, 2020.
- ³¹Tomaiuolo, M., C. N. Matzko, I. Poventud-Fuentes, J. W. Weisel, L. F. Brass, and T. J. Stalker. Interrelationships between structure and function during the hemostatic response to injury. *Proc. Natl. Acad. Sci. USA.* 116:2243–2252, 2019.
- ³²van Nieuwkoop, C. COVID-19 associated pulmonary thrombosis. *Thromb. Res.* 191:151, 2020.
- ³³Welsh, J. D., I. Poventud-Fuentes, S. Sampietro, S. L. Diamond, T. J. Stalker, and L. F. Brass. Hierarchical organization of the hemostatic response to penetrating injuries in the mouse macrovasculature. *J. Thromb. Haemost.* 15:526–537, 2017.
- ³⁴Ye, Q., B. Wang, and J. Mao. The pathogenesis and treatment of the 'Cytokine Storm' in COVID-19. *J. Infect.* 80:607–613, 2020.
- ³⁵Younan, X., and G. M. Whitesides. Soft lithography. *Annu. Rev. Mater. Sci.* 28:153–184, 1998.

- ³⁶Zilberman-Rudenko, J., J. L. Sylman, H. H. S. Lakshmanan, O. J. T. McCarty, and J. Maddala. Dynamics of blood flow and thrombus formation in a multi-bypass microfluidic ladder network. *Cell Mol. Bioeng.* 10:16–29, 2017.
- ³⁷Zilberman-Rudenko, J., R. M. White, D. A. Zilberman, H. H. S. Lakshmanan, R. A. Rigg, J. J. Shatzel, J. Maddala, and O. J. T. McCarty. Design and utility of a point-of-care

microfluidic platform to assess hematocrit and blood coagulation. *Cell Mol. Bioeng.* 11:519–529, 2018.

Publisher's Note Springer Nature remains neutral with regard to jurisdictional claims in published maps and institutional affiliations.